Neuron
Article

Mechanism of ER Stress-Induced Brain Damage by IP_3 Receptor

Takayasu Higo,[1,2,8] Kozo Hamada,[2,5] Chihiro Hisatsune,[2] Nobuyuki Nukina,[3] Tsutomu Hashikawa,[4] Mitsuharu Hattori,[6] Takeshi Nakamura,[7,9] and Katsuhiko Mikoshiba[1,2,5,*]
[1]Department of Molecular Neurobiology, Institute of Medical Science, University of Tokyo, 4-6-1 Shirokanedai, Minato-ku, Tokyo 108-8639, Japan
[2]Laboratory for Developmental Neurobiology
[3]Laboratory for Structural Neuropathology
[4]Laboratory for Neural Architecture
Brain Science Institute, RIKEN, Wako, Saitama 351-0198, Japan
[5]Calcium Oscillation Project, ICORP-SORST, JST, 4-1-8 Honcho, Kawaguchi, Saitama 332-0012, Japan
[6]Department of Biomedical Science, Graduate School of Pharmaceutical Sciences, Nagoya City University, Mizuho-ku, Nagoya, Aichi 467-8603, Japan
[7]Department of Physiology, Juntendo University School of Medicine, Bunkyo-ku, Tokyo 113-8421, Japan
[8]Present address: Laboratory for Cognitive Brain Mapping, Brain Science Institute, RIKEN, Wako, Saitama 351-0198, Japan
[9]Deceased
*Correspondence: mikosiba@brain.riken.jp
DOI 10.1016/j.neuron.2010.11.010

SUMMARY

Deranged Ca^{2+} signaling and an accumulation of aberrant proteins cause endoplasmic reticulum (ER) stress, which is a hallmark of cell death implicated in many neurodegenerative diseases. However, the underlying mechanisms are elusive. Here, we report that dysfunction of an ER-resident Ca^{2+} channel, inositol 1,4,5-trisphosphate receptor (IP_3R), promotes cell death during ER stress. Heterozygous knockout of brain-dominant type1 IP_3R (IP_3R1) resulted in neuronal vulnerability to ER stress in vivo, and IP_3R1 knockdown enhanced ER stress-induced apoptosis via mitochondria in cultured cells. The IP_3R1 tetrameric assembly was positively regulated by the ER chaperone GRP78 in an energy-dependent manner. ER stress induced IP_3R1 dysfunction through an impaired IP_3R1-GRP78 interaction, which has also been observed in the brain of Huntington's disease model mice. These results suggest that IP_3R1 senses ER stress through GRP78 to alter the Ca^{2+} signal to promote neuronal cell death implicated in neurodegenerative diseases.

INTRODUCTION

Two common signs of neurodegenerative diseases such as Alzheimer's disease and Huntington's disease (HD) are the aggregation of aberrant misfolded proteins and deranged Ca^{2+} signaling (Schröder and Kaufman, 2005; Kim et al., 2008). The most important organelle to prevent misfolded protein accumulation is the endoplasmic reticulum (ER), which strictly controls protein quality (Ellgaard and Helenius, 2003; Schröder and Kaufman, 2005). However, when the capacity of the quality control system is exceeded, ER undergoes severe stress and induces cell death implicated in neurodegenerative diseases (Schröder and Kaufman, 2005; Kim et al., 2008). An ER chaperone, GRP78, acts as the master regulator of unfolded protein response (UPR) signaling to improve biogenetic processes and has a cytoprotective function against ER stress (Hendershot, 2004; Mimura et al., 2007; Wang et al., 2010). Genetic studies have shown that the loss of GRP78 function leads to defective neural development and involuntary movement (Mimura et al., 2007; Wang et al., 2010). A recent study indicates that the three branches of UPR signaling (IRE1, PERK, and ATF6) regulate cell death in response to prolonged ER stress (Lin et al., 2007). While these branches do not directly cause cell death, they do initiate activation of downstream factors at transcriptional levels (Schröder and Kaufman, 2005; Li et al., 2006; Kim et al., 2008). ER stress also alters Ca^{2+} mobilization to activate apoptosis (Schröder and Kaufman, 2005; Kim et al., 2008), in which the proapoptotic factors BAX and BAK are translocated from ER to mitochondria (Scorrano et al., 2003). However, the mechanisms of Ca^{2+}-dependent apoptosis executed during ER stress are poorly understood.

ER functions as a major intracellular Ca^{2+} store involved in Ca^{2+} signaling and homeostasis (Berridge et al., 2003). The inositol 1,4,5-trisphosphate receptors (IP_3Rs) are ER-resident Ca^{2+} release channels that play critical roles in Ca^{2+} signaling. There are three subtypes of IP_3R (IP_3R1, IP_3R2, and IP_3R3), each of which has a distinct physiological property (Mikoshiba, 2007). IP_3R1 is expressed ubiquitously. In particular, it is the predominant subtype in the cerebellum and regulates synaptic plasticity (Mikoshiba, 2007). Genetic studies have shown that ablation of IP_3R1 can cause a movement disorder (Matsumoto et al., 1996) and is a causative factor in the development of spinocerebellar ataxia type 15, categorized as a neurodegenerative disease (Hara et al., 2008). However, the results of physiological studies differ regarding the roles of IP_3R1 during

apoptotic events (Sugawara et al., 1997; Blackshaw et al., 2000; Boehning et al., 2003; Mendes et al., 2005).

All three subtypes have a cytosolic region including an IP_3-binding core in the N-terminal portion and a channel domain at the extreme C-terminal end. These subtypes can form either a homotetramer or heterotetramer with each having distinct channel properties (Thrower et al., 2001; Mikoshiba, 2007). These various intrinsic channel properties enable them to generate diverse patterns of Ca^{2+} signals, which presumably have profound effects on cellular processes (Sugawara et al., 1997; Thrower et al., 2001). Thus, it is important to understand the molecular mechanism of the IP_3R subunit assembly, but the mechanisms have not been explored. In addition to cytosolic factors including IP_3 and its associated proteins (Mikoshiba, 2007), IP_3R1 is regulated by an ER lumenal protein through interactions with the largest lumenal loop (L3) in the channel domain containing six transmembrane domains (TM1–TM6) (Higo et al., 2005). L3 is segmented between TM5 and TM6 and includes two characteristic regions. The first half has a divergent region among all subtypes (L3V), and the second half contains the pore-forming region, which is completely conserved among subtypes (L3C) (Higo et al., 2005). We have shown that L3V is important for subtype-specific regulation of IP_3R, and it also functions as the lumenal sensor for environmental changes leading to ER stress (Higo et al., 2005). However, it is unknown whether and how IP_3R1 regulates ER stress-dependent neuronal cell death.

RESULTS

Loss of IP_3R1 Enhances Neuronal Vulnerability to ER Stress

To examine the significance of IP_3R1 in ER stress-induced cell death in vivo, we used heterozygous (+/−) knockout ($IP_3R1^{+/-}$) mice (Figure 1A) showing normal growth but not homozygous (−/−) mice, which died three weeks after birth (Matsumoto et al., 1996). Mice were intraperitoneally injected with an ER stressor tunicamycin (Tun, an inhibitor of N-linked glycosylation) and were killed 48 hr after injection. This procedure has been validated as an in vivo model for ER stress (Hetz et al., 2006). Hematoxylin and eosin staining revealed that at 48 hr after injection, heterozygous knockout mice had more pyknotic Purkinje neurons than wild-type (WT, $IP_3R1^{+/+}$) mice (Figure 1B). Heterozygous knockout mice also exhibited a significant reduction in calbindin signals in the cerebellum compared to WT mice (Figure 1C). These results suggest that the loss of IP_3R1 function caused the neural damages under ER stress conditions.

To further investigate a physiological role of IP_3R1 in ER stress-induced cell death, we knocked down IP_3R1 expression using small interfering RNA (siRNA) in HeLa cells dominantly expressing IP_3R1 (Hattori et al., 2004). We monitored the effects of IP_3R1 knockdown on apoptosis over time after treatment of various ER stressors Tu, or dithiothreitol (DTT, a reducing agent), or thapsigargin (Tg, an ER Ca^{2+}-ATPase inhibitor). Annexin-V/propidium iodide staining showed that IP_3R1 knockdown significantly enhanced ER stress-induced apoptosis at 24 hr and 48 hr time periods (Figures 1D, and see Figure S1A available online). To further understand this underlying mechanism of apoptosis enhanced by the loss of IP_3R1 function, we analyzed the time course of the effect of IP_3R1 knockdown on three branches of the UPR signaling. IP_3R1 knockdown did not alter the splicing of XBP-1 (Figure S1B), the cleavage of ATF6 (Figure S1C), or induced expression of GRP78 and ATF4 during ER stress (Figure S1C). These results suggest an irrelevance in the role of IP_3R1 in the UPR signaling that regulates ER stress-induced apoptosis.

IP_3R-mediated Ca^{2+} release from ER and mitochondrial Ca^{2+} homeostasis are physiologically coupled to affect cell viability (Joseph and Hajnóczky, 2007). We therefore examined an involvement of IP_3R1 in apoptosis via mitochondria using a fluorescent cationic dye, MitoCapure, which enables us to assess the lowered mitochondrial potential and the subsequent apoptosis (Matassa et al., 2001). IP_3R1 knockdown significantly increased the number of cells fluorescing green at 24 hr and 48 hr time periods of ER stress (Figures 1E and S1D), indicating the IP_3R1 knockdown lowered mitochondria membrane potential to enhance apoptosis during ER stress. The significance of IP_3R1 in mitochondria-dependent apoptosis in response to ER stress was further reinforced by enhancement of released cytochorome c in IP_3R1 knockdown cells (Figure S1E).

These results from loss-of-function approaches prompted us to ask whether IP_3R1 function was impaired under ER stress conditions that execute cell death. To test this possibility, we performed Ca^{2+}-imaging experiments using N1E-115 mouse neuroblastoma cells, which substantially expressed only IP_3R1 (Figures S2A–S2C; Fink et al., 2000). Ca^{2+} imaging revealed that treatment with ER stressors significantly inhibited IP_3R1-mediated Ca^{2+} release (Figure 2A). Using Tg, we excluded the possibility that the inhibitory effect on Ca^{2+} release was due to decreased ER Ca^{2+} content (Figure S2D). Attenuated IP_3-induced Ca^{2+} release was also obtained in HeLa cells (Figures 2B and S2E). Furthermore, using microsomal fractions from cells treated with DTT or Tun, we have clearly demonstrated that ER stress impaired IP_3R1 channel activity (Figure 2C). This attenuated channel activity of IP_3R1 was also ascertained using primary neurons (Figure 2D).

GRP78 Subtype Specifically Binds to IP_3R1

To explore a molecular mechanism underlying the disrupted function of IP_3R1 during ER stress, we first searched for ER proteins that bound to L3V (Figure 3A) under normal (nonreduction) and ER stress conditions (reduction). In glutathione S-transferase (GST) pull-down experiments, we found a protein of approximately 75 kDa, which precipitated with IP_3R1-L3V (1L3V) under only normal conditions (Figure S3A) and identified it as GRP78 by mass spectrometry (Figure S3B). GRP78 was identified as neither an IP_3R2- nor an IP_3R3-associated protein (data not shown). GST pull-down experiments revealed that GRP78 directly and subtype-specifically interacted with IP_3R1 (Figure 3B).

Next, we investigated the interaction of IP_3R1 with GRP78 in living cells. Immunocytochemistry showed that IP_3R1 and GRP78 were colocalized in ER (Figure 3C). Immunoprecipitation (IP) experiments using HeLa cell lysates revealed that IP_3R1 and GRP78 were present in the same complexes (Figure 3D). There is another ER chaperone ERp44 that binds to 1L3V under reduced conditions (Higo et al., 2005). Therefore, we examined the effect

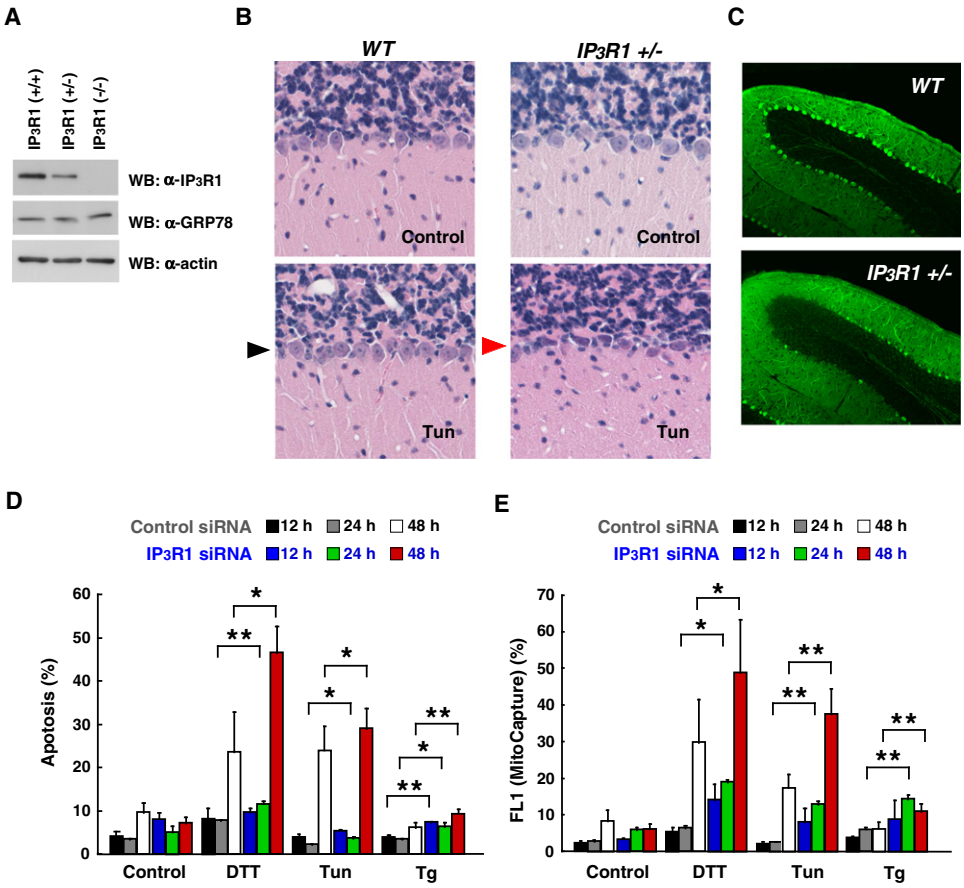

Figure 1. The Loss of IP_3R1 Function Enhances ER Stress-Induced Neuronal Death

(A) Expression levels of IP_3R1 and an ER lumenal protein, GRP78, in crude microsome prepared from cerebella of IP_3R1 (+/+), IP_3R1 (+/−), and IP_3R1 (−/−) mice.

(B and C) In vivo effect of ER stress on Purkinje neurons in wild-type (WT) and heterozygous IP_3R1 knockout mice ($IP_3R1^{+/-}$). Representative hematoxylin and eosin (HE)-stained (B) and α-calbindin-stained (C) cerebellum sections from WT and $IP_3R1^{+/-}$ mice sacrificed 2 days after injection of Tun (1 μg/g) or control phosphate-buffered saline. Note marked increase of shrunken neurons (B) and decrease of calbindin signals (C) in the cerebellum lobule VI of $IP_3R1^{+/-}$. Arrowheads indicate Purkinje cell layer in WT (black) and $IP_3R1^{+/-}$ (red). We confirmed reproducibility using five and two littermate pairs (WT and $IP_3R1^{+/-}$) for HE staining and for calbindin immunostaining, respectively.

(D and E) Enhancements of apoptosis by IP_3R1 knockdown. HeLa cells transfected with IP_3R1 siRNA were treated with Tun (5 μg/ml) or Tg (2 μM) or DTT (2 mM) for 12, 24, or 48 hr. The cells were stained with Annexin-V FITC/PI (D) or MitoCapture (E). (D) The percentage of apoptosis (Annexin-positive/PI-negative) in at least 10,000 cells was determined by flow cytometer analysis, in which the cells treated with 1 μM staurosporine for 4 hr were used as a positive-control. (E) A cationic MitoCapture dye selectively enters into mitochondria to fluoresce red in healthy cells, and changes reversely its color from red to green (FL1) as membrane potential decreases in apoptotic cells. The percentage of cells showing a green fluorescence (FL1) in at least 10,000 cells was determined by flow cytometer analysis. Data in (D) and (E) are presented as mean ± SEM from at least three independent experiments. *$p < 0.05$; **$p < 0.005$.

See also Figure S1.

of GRP78 on IP_3R1-ERp44 interaction. Coexpression of GRP78 decreased IP_3R1 immunoprecipitated with ERp44 (Figure 3E), indicating that GRP78 outcompetes binding of ERp44 to IP_3R1 under normal conditions. Furthermore, we examined the interaction of IP_3R1 with GRP78 in the brain. Immunohistochemistory experiments showed that IP_3R1 and GRP78 were colocalized in the cortex and striatum (Figure 3F). Moreover, IP experiments showed that IP_3R1 and GRP78 were in the same complexes in the brain homogenates and primary cortical neurons of the mice (Figures 3G and 3H). These results indicate that IP_3R1 interacts with GRP78 in vivo.

Finally, to examine the interaction between IP_3R1 and GRP78 during ER stress, IP experiments were performed using cell lysates treated with various ER stressors. Although treatment with these agents did not attenuate IP_3R1 expression, the quantity of IP_3R1 that immunoprecipitated with GRP78 decreased (Figure 3I). These results are further reinforced by the attenuated interaction in the brain of mice intraperitoneally injected with Tun (Figure 3J).

Interaction of IP_3R1 with GRP78 Is Impaired in Huntington's Disease Model Mice

To investigate the involvement of the IP_3R1-GRP78 interaction in neurodegenerative diseases associated with ER stress and deranged Ca^{2+} homeostasis (Schröder and Kaufman, 2005; Kim et al., 2008), we focused on HD caused by pathologically

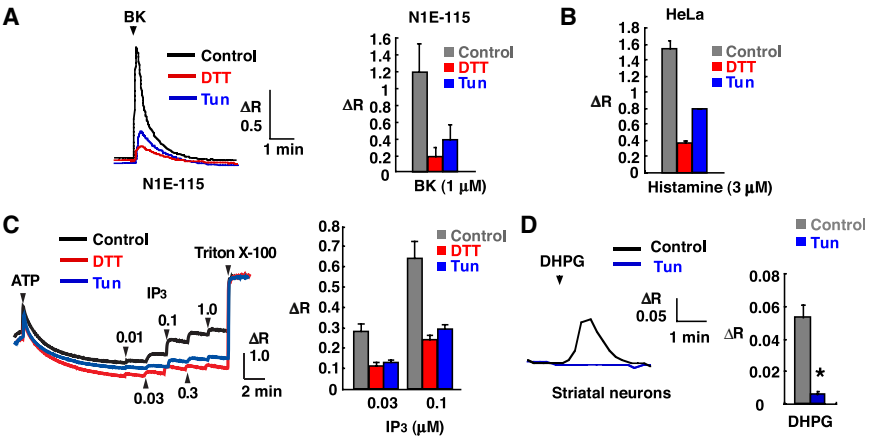

Figure 2. ER Stress Impairs IP_3R1-Mediated Ca^{2+} Release

(A and B) Representative Ca^{2+} responses in N1E-115 cells treated with control DMSO (black), DTT (red), or Tun (blue) for 16 hr are shown in (a, left traces). N1E-115 (A) and HeLa (B) cells were stimulated with 1 μM bradykinin (BK) and 3 μM histamine in the absence of extracellular Ca^{2+}, respectively. Bar charts summarize average peak amplitude of Ca^{2+} release in N1E-115 (A) and HeLa (B) cells treated with control DMSO (gray), DTT (red), or Tun (blue).

(C) ER stress attenuates IP_3-induced Ca^{2+} release. After ATP-dependent uptake of Ca^{2+} into crude microsomes from HeLa cells pretreated with DMSO (black), DTT (red), or Tun (blue), for 48 hr, the indicated concentrations of IP_3 (μM) were sequentially added.

(D) ER stress impairs IP_3R1-mediated Ca^{2+} release in primary neurons. Primary striatal neurons were treated with Tun (5 μg/ml) for 12 hr and then stimulated with 100 μM 3,5-dihydroxyphenylglycine (DHPG), a specific agonist for group 1 and 5 metabotropic glutamate receptors, after depolarization with 30 mM KCl to fill the Ca^{2+} store. Data are presented from at least three independent experiments. Data in (A) to (D) are presented as mean ± SEM from at least three independent experiments. *$p < 0.05$.

See also Figure S2.

expanded polyglutamine (Kim et al., 2008; Vonsattel, 2008) and employed the model mouse R6/2 that expresses exon1 of the human Huntington gene with an expanded CAG repeat (Vonsattel, 2008). Pathologically, the affected regions are not limited in the striatum but are spread to the cerebral cortex in HD (Vonsattel, 2008). Therefore, we first performed IP experiments to examine IP_3R1-GRP78 interaction in cerebrum of the model mice. Coprecipitation of GRP78 with immunoprecipitated IP_3R1 decreased more significantly in the homogenates from the model mice relative to those from WT mice (Figure 4A).

Next, we examined the interaction in the striatum. IP experiments revealed decreased interaction in the model mice (Figure 4B), consistent with the decreased interaction in the cerebrum (Figure 4A). Moreover, using primary striatal neurons, we assessed the channel activity of IP_3R1 in the model. Ca^{2+}-imaging experiments showed that IP_3R1 activity significantly decreased compared to WT mice (Figure 4C). Similarly, decreased interaction and attenuated IP_3R1 activity were obtained from the cerebellum of the model mice (Figures 4D and 4E).

GRP78 Is Required for IP_3R1 Channel Function but Not for That of IP_3R2 or IP_3R3

To investigate the role of endogenous GRP78 in IP_3R1 channel activity in living cells, we knocked down GRP78 expression using siRNA in HeLa and COS-7 cells. HeLa cells dominantly express IP_3R1 and IP_3R3, whereas COS-7 cells express IP_3R2 and IP_3R3 (Hattori et al., 2004). GRP78 expression was knocked down using siRNA against human GRP78 without interfering with the expression levels of IP_3R or other ER proteins in either cell line (Figure 5A). Ca^{2+} imaging was performed to monitor agonist-induced Ca^{2+} release to evaluate the role of GRP78 on IP_3R1 channel activity. Control of GRP78 siRNA-transfected HeLa cells was stimulated by stepwise increasing concentrations of an agonist, ATP (Figure 5B, black and red traces). GRP78 suppression significantly decreased the average peak amplitude (Figures 5B and 5C, red trace and bar) and the number of responsive cells (Figure S4A, red bar) compared to control cells (Figures 5B and 5C and Figure S4A, black trace and gray bar).

The inhibitory effect of GRP78 knockdown on the Ca^{2+} signal was also obtained by a different agonist, histamine (Figure S4B) and by ectopic expression of ER targeted-1L3V that can work as a dominant-negative by competing endogenous IP_3R1 (Figures S4C and S4D). In contrast, GRP78 suppression had no effect on agonist-induced Ca^{2+} release in COS-7 cells (Figures 5D, 5E, and S4E), indicating that GRP78 does not regulate IP_3R2, IP_3R3 or other proteins involved in IP_3 production. We used N1E-115 cells to confirm the specific effect of GRP78 on IP_3R1. GRP78 knockdown significantly inhibited IP_3R1-mediated Ca^{2+} release in this cell line (Figures 5F–5H). We discharged the Ca^{2+} stores using Tg to exclude the possibility that these inhibitory effects obtained in N1E-115 and HeLa cells were due to decreased Ca^{2+} contents in ER. A reduction in Ca^{2+} leakage was not observed in GRP78 siRNA-transfected cells when compared to the control (Figures 5I and S4F). Finally, in order to confirm the effect of GRP78 knockdown, GRP78 expression was reintroduced into HeLa cells in which GRP78 was knocked down. Re-expression of GRP78 restored the attenuated Ca^{2+} release (Figures 5J). Therefore, we concluded that GRP78 was required for IP_3R1 channel activity.

GRP78 Is Required for the Tetrameric Assembly of IP_3R1

We explored the underlying mechanism of channel regulation by GRP78. GRP78 knockdown and deletion of 1L3V did not affect IP_3R1 subcellular localization (Figures S5A and S5B). These results indicate that IP_3R1 could be properly folded, because misfolded proteins are retrotranslocated to the cytosol (Ellgaard and Helenius, 2003; Parker et al., 2004). Likewise, GRP78 knockdown did not alter IP_3R1 sensitivity to endoglycosidase H (Figure S5C), suggesting that 1L3V normally undergoes both an N-linked glycosylation and topological organization.

To examine whether GRP78 regulates the IP_3R1 subunit assembly, we evaluated the effect of GRP78 expression on IP_3R1 assembly status, including the monomer, intermediates,

and the tetramer. First, siRNA-transfected HeLa cells were treated with a crosslinker, DSP, to preserve the IP_3R1 complex, and the cell lysates were solubilized with Triton X-100 and subjected to gel filtration. In the control, IP_3R1 eluted in fractions corresponding to 1000–2000 kDa (Figures 6A and S5D), whereas GRP78 knockdown substantially shifted IP_3R1 to lower molecular weight fractions (Figure 6A). We also ran a set of standards to create a calibration curve and determine the precise size of the proteins (Figure 6B). Based on the IP_3R1 elution profiles and densitometric analysis, the averaged peaks of eluted IP_3R1 in the control and in the GRP78 knockdown cells were fractions 12 and 15, respectively (Figure 6C). The calibration curve indicated apparent IP_3R1 molecular masses of approximately 1.2 MDa and 660 kDa in fractions 12 and 15, respectively. Therefore, these results revealed that GRP78 knockdown reduces the size of the IP_3R1 complex by approximately 50% in HeLa cells. Similar results were obtained in N1E-115 cells (Figure 6D). In contrast, GRP78 knockdown did not affect IP_3R2 or IP_3R3 distributions in the fractionation of HeLa (Figures 6A and S5D) or COS-7 cells (Figure 6E).

We hypothesized that ER stress impaired the IP_3R1 tetrameric assembly. To test this, gel filtration was performed using the lysates from HeLa cells treated with ER stressors. Consistent with the inhibitory effects of ER stress on IP_3R1 channel activity (Figures 2A–2D) and the interaction of IP_3R1 with GRP78 (Figures 3I and 3J), the subunit assembly was inhibited by ER stress (Figure 6F), and the effects were ameliorated by GRP78 overexpression (Figure 6G).

We next employed sucrose density gradient sedimentation. IP_3R1 was mainly detected in fractions 13 to 15 in the control (Figure 7A, top), whereas GRP78 knockdown caused a diffuse distribution encompassing the monomer and intermediates from top to bottom in the gradient (Figure 7A). The subtype-specific effect of GRP78 knockdown on IP_3R assembly was also confirmed using the N1E-115 lysates (Figure 7B, top). Consistent with the gel filtration results, GRP78 knockdown had no effect on IP_3R3 distribution in the gradients of HeLa (Figure 7A, middle) or COS-7 cells (Figure 7B, middle). Moreover, the significance of GRP78 binding to 1L3V in the IP_3R1 assembly was assessed using an L3V-deleted mutant of green fluorescent protein-tagged IP_3R1 (Figure 7B, bottom). These subtype-specific effects of GRP78 knockdown on both the size and density of IP_3R1 strongly support the idea that GRP78 regulates the IP_3R1 subunit assembly.

To further investigate the assembly status of IP_3R1 under GRP78-deleted conditions, the HeLa cell lysates crosslinked with a noncleavage crosslinker, DSS, were separated on 5%–20% sucrose gradients, and the resultant fractions were resolved on native polyacrylamide gel electrophoresis (PAGE). Most IP_3R1 presented in fractions 13–15 of the control and migrated near the top of the gel. The apparent size of IP_3R1 in those fractions was larger than 669 kDa (Figure 7C, left panel). GRP78 knockdown shifted IP_3R1 to fractions 7 and 9, which are equivalent to the monomer and intermediates (Figure 7C, right panel).

Pulse labeling was performed to clarify the role of GRP78 in IP_3R1 assembly (Figure 7D). HeLa cells transfected with GRP78 siRNA were labeled with ^{35}S-methionine, lysates were loaded on sucrose gradients, and the resultant fractions were immunoprecipitated. In the control, radioactivity was primarily detected among the fractions containing tetrameric IP_3R1 (Figure 7E), whereas GRP78 knockdown increased the relative degree of radioactivity in the fractions containing the intermediate monomer (Figure 7E). In contrast, the distribution of ^{35}S-labeled IP_3R3 was unaffected by GRP78 knockdown (Figure 7E).

GRP78 Regulates Tetrameric Assembly of IP_3R1 Depending on Its ATPase Activity

We further investigated the regulatory mechanism of IP_3R1 by GRP78. GRP78 has ATPase activity and stably binds to the chaperone substrate in ADP and releases it in ATP (Misselwitz et al., 1998; Hendershot, 2004). Using a surface plasmon resonance assay, we examined the real-time interaction between the two proteins. Unexpectedly, GRP78 showed enhanced interaction with 1L3V in ATP compared to that in ADP (Figure 8A). Moreover, GRP78 showed a relatively robust interaction with IP_3R1 in the presence of ATP compared to that of a typical GRP78-binding peptide, P15 (Misselwitz et al., 1998; Nawa et al., 2007; Figure 8A). To examine the ATP-dependent interaction of IP_3R1 with GRP78 in vivo, we used the well-characterized T37G ATPase mutant, which can bind to ATP but does not undergo an ATP-induced conformational change (Wei et al., 1995). IP experiments revealed that the mutant interacted with IP_3R1 as well as the WT counterpart (Figure 8B). Gel filtration was then performed to examine the significance of the ATPase activity of GRP78 in the tetrameric assembly of IP_3R1. Unlike GRP78 WT, T37G expression inhibited the tetrameric assembly of IP_3R1 (Figure 8C). Ca^{2+} imaging was performed to confirm the effect of ATPase mutants on IP_3R1 channel activity. While GRP78 overexpression significantly enhanced IP_3R-mediated Ca^{2+} release (Figures 8D and 8E, red trace and red bar) without affecting ER Ca^{2+} content (Figure 8F), T37G failed to enhance Ca^{2+} release and generated more oscillatory Ca^{2+} responses (Figures 8D, 8E, and S6). Similar effects were observed in cells expressing other ATPase mutants, G226D and Delta A (Gaut and Hendershot, 1993; Wei et al., 1995; Figures 8D, 8E, and S6). Finally, the facilitative effect of GRP78 WT on IP_3R1 was confirmed using primary cortical neurons (Figures 8G and 8H). Taken together, results from the biochemical and Ca^{2+}-imaging experiments show that the tetrameric assembly of IP_3R1 is energy and ER stress dependently regulated by GRP78.

DISCUSSION

Our study demonstrated a novel regulatory mechanism of IP_3R-Ca^{2+} signaling in which IP_3R1 is positively regulated by GRP78 from the ER lumen. Under nonstressed conditions, this mechanism ensures intracellular Ca^{2+} signaling, which is essential for various cellular processes for cell survival (Berridge et al., 2003; Mikoshiba, 2007). In contrast, ER stress impairs this mechanism, causing attenuation of IP_3R1 activity. Our results indicate that loss of IP_3R1 function lowers the mitochondrial membrane potential to promote apoptosis via mitochondria. Since IP_3R-mediated Ca^{2+} release from ER and Ca^{2+} uptake

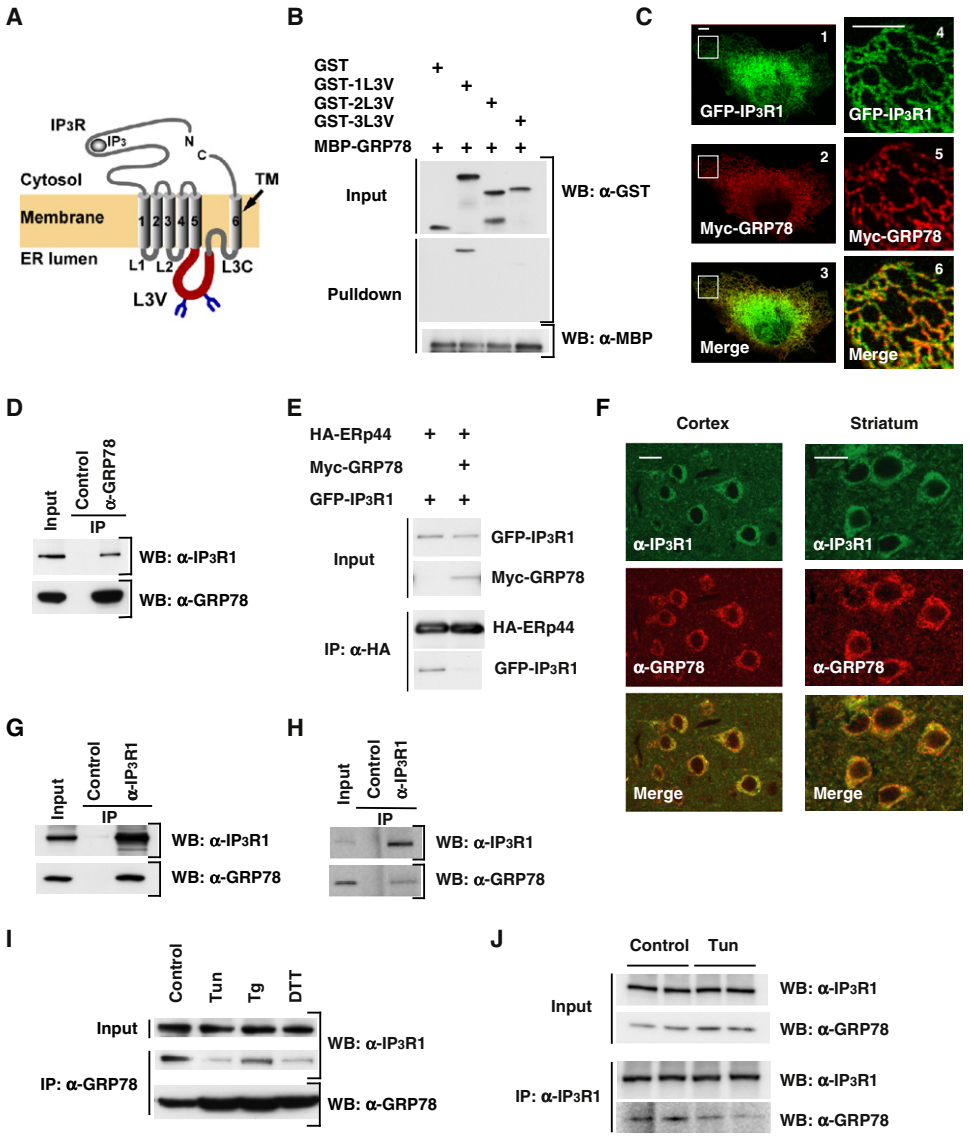

Figure 3. Identification of GRP78 as an IP_3R1-Associated Protein

(A) Schematic representation of IP_3R. IP_3R contains six transmembrane domains (TMs) and three lumenal loops, L1, L2, and L3. L3 is divided into L3V (red) with two glycosylations (blue) and L3C. IP_3 binds to the N-terminal cytosolic region.

(B) GRP78 specifically interacts with the L3V of IP_3R1, but not that of IP_3R2 or IP_3R3. Purified GST, GST-1L3V, GST-2L3V, or GST-3L3V was incubated with maltose-binding protein (MBP)-GRP78. Protein complexes were isolated using amylose resin and analyzed by western blotting with α-GST (top and middle) or α-MBP (bottom).

(C) GRP78 colocalizes with IP_3R1 in ER. COS-7 cells expressing Myc-GRP78 and green fluorescent protein-tagged IP_3R1 (GFP-IP_3R1) were stained with α-Myc (panels 1–3). The boxed regions in panels 1–3 are shown at increased magnification in panels 4–6, respectively. Scale bar, 5 μm.

(D) In vivo interaction between GRP78 and IP_3R1. HeLa cells were treated with a membrane-permeable crosslinker, DSP, and the cell lysates were subjected to immunoprecipitation (IP) with control rabbit IgG or α-GRP78. The lysate (Input) and IP samples were analyzed as in (B).

(E) GRP78 inhibits binding of ERp44 to IP_3R1. COS-7 cells were transfected with expression vectors for GFP-IP_3R1 and HA-ERp44 or GFP-IP_3R1, HA-ERp44, and Myc-GRP78. Forty-eight hours after transfection, cells were treated with DSP for 30 min. After washing with PBS, the cells were solubilized and then subjected to IP with α-HA (3F10). The lysate (Input) and IP samples were analyzed as in (D).

(F) GRP78 colocalizes with IP_3R1 in the brain. Mouse cortical and striatal sections were immunostained with α-IP_3R1 and α-GRP78. Scale bar, 10 μm.

(G and H) Interaction of IP_3R1 with GRP78 in the brain. (G) Crude microsome obtained from P14 mouse brain was solubilized and the cleared fraction was immunoprecipitated with α-IP_3R1 (10A6). The lysate (Input) and IP samples were analyzed as described above. (H) Primary cortical neurons were treated with DSP and the cell lysates were subjected to IP and then analyzed as in (G).

(I and J) ER stress inhibits the interaction of IP_3R1 with GRP78. (I) HeLa cells were treated with DMSO, Tun (2 μg/ml), Tg (2 μM), and DTT (2 mM) for 24 hr. After cross-linking with DSP, the cell lysates were subjected to IP with α-IP_3R1. (J) Forty-eight hours after Tun injection to P14 mice, the cerebra were

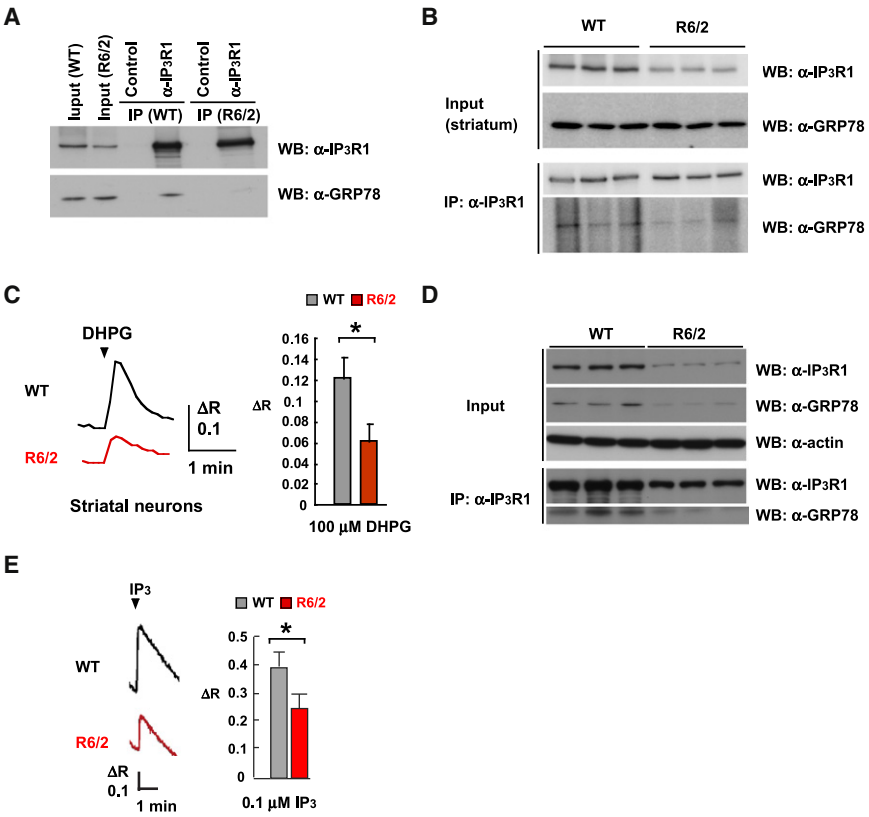

Figure 4. IP_3R1-GRP78 Interaction Is Inhibited in the Model Mice of the Huntington's Disease

(A) IP_3R1 and GRP78 interaction in model mice of Huntington's disease (HD). Crude microsome fraction was obtained from cerebrum of WT or R6/2 mice (8 weeks) that have been widely used as a model mouse of HD. The detergent-solubilized fractions (Input) were immunoprecipitated with α-IP_3R1 (10A6) and the IP samples were analyzed by western blotting.

(B) Decreased interaction of IP_3R1 with GRP78 in the HD model mice. The homogenates of the R6/2 mice striatum were solubilized and the cleared fraction was immunoprecipitated with α-IP_3R1. The lysate (Input) and IP samples were analyzed as described above.

(C) Impaired Ca^{2+} release activity of IP_3R1 in the striatum of HD model mice. Primary striatal neurons were stimulated with 100 μM DHPG after depolarization with 30 mM KCl.

(D) Decreased interaction of IP_3R1 with GRP78 in the HD model mice. Crude microsome fraction was obtained from cerebellum of WT or R6/2 mice. The detergent-solubilized fractions (Input) were immunoprecipitated with α-IP_3R1 (10A6) and the IP samples were analyzed as in (B). The ratio of the densities of the IP samples (GRP78/IP_3R1) in WT and R6/2 are 0.35 ± 0.03 (mean ± standard error of mean [SEM], n = 3) and 0.21 ± 0.05 (mean ± SEM, n = 3) respectively, and these results show the significant reduction in interaction of the two proteins in the cerebellum of R6/2 mice compared with that in WT ($p < 0.05$).

(E) Impaired Ca^{2+} release activity of IP_3R1 in the cerebellum of HD model mice. Ca^{2+} uptake into the microsomes obtained from cerebellum of WT or R6/2 mice was initiated by addition of ATP and then 0.1 μM IP_3 was added to monitor IP_3R1 activity. Data in (C) and (E) are presented as mean ± SEM from at least three independent experiments. *$p < 0.05$.

into mitochondria are tightly coupled (Joseph and Hajnóczky, 2007), ER stress-dependent impairment of IP_3-Ca^{2+} signaling attenuate mitochondrial Ca^{2+} uptake (Biagioli et al., 2008), and the resultant reduced mitochondrial Ca^{2+} lowers the membrane potential (Zhu et al., 1999), and decrease of the membrane potential in mitochondria attenuates IP_3R-mediated Ca^{2+} release (Collins et al., 2000). Thus, our finding reasonably supports a possibility that the levels of mitochondrial Ca^{2+} and the membrane potential during ER stress progressively fall by the positive feedback loop below the threshold required for cell survive (Zhu et al., 1999), which would lead to further activation of the apoptotic pathways.

While much of the literature has addressed the relationship between augmented release of Ca^{2+} via IP_3R and mitochondria-dependent apoptosis (Boehning et al., 2003; Joseph and Hajnóczky, 2007), our study is the first to highlight the significance of reduced IP_3-mediated Ca^{2+} signal in apoptosis, in particular, during ER stress, and further uncovers the underlying mechanisms of mitochondria-dependent apoptosis when intracellular Ca^{2+} concentration is out of physiological range. In addition, this IP_3R1 dysfunction-dependent apoptotic pathway would be different from the canonical three branches of UPR signaling that regulates cell fate (Lin et al., 2007), and is likely to be specified for the apoptosis under deranged Ca^{2+} conditions caused by ER stress.

Our results show that functional interaction of IP_3R1 with GRP78 and the channel activity of IP_3R1 are impaired in the cortex and striatum of the HD model mice. Our study supports a possibility that impairment of IP_3R1 function promotes mitochondria-dependent cell death in the model mice by producing negative effects on mitochondrial Ca^{2+} and the membrane potential. This is consistent with a previous study which showed that expanded polyglutamine contributory to ER stress reduced the mitochondria membrane potential and significantly decreased the mitochondrial Ca^{2+} uptake (Panov et al., 2002). Moreover, HD patients and the mouse model showed impairments in mitochondrial ATP production (Seong et al., 2005), and mitochondrial dysfunction has long been proposed to contribute to HD pathogenesis (Bossy-Wetzel et al., 2008). One may speculate that mitochondrial dysfunction reduces

dissected and homogenized. The crude microsome was solubilized and the cleared fractions were immunoprecipitated with α-IP_3R1. The lysate (Input) and IP samples were analyzed as in (G).
See also Figure S3.

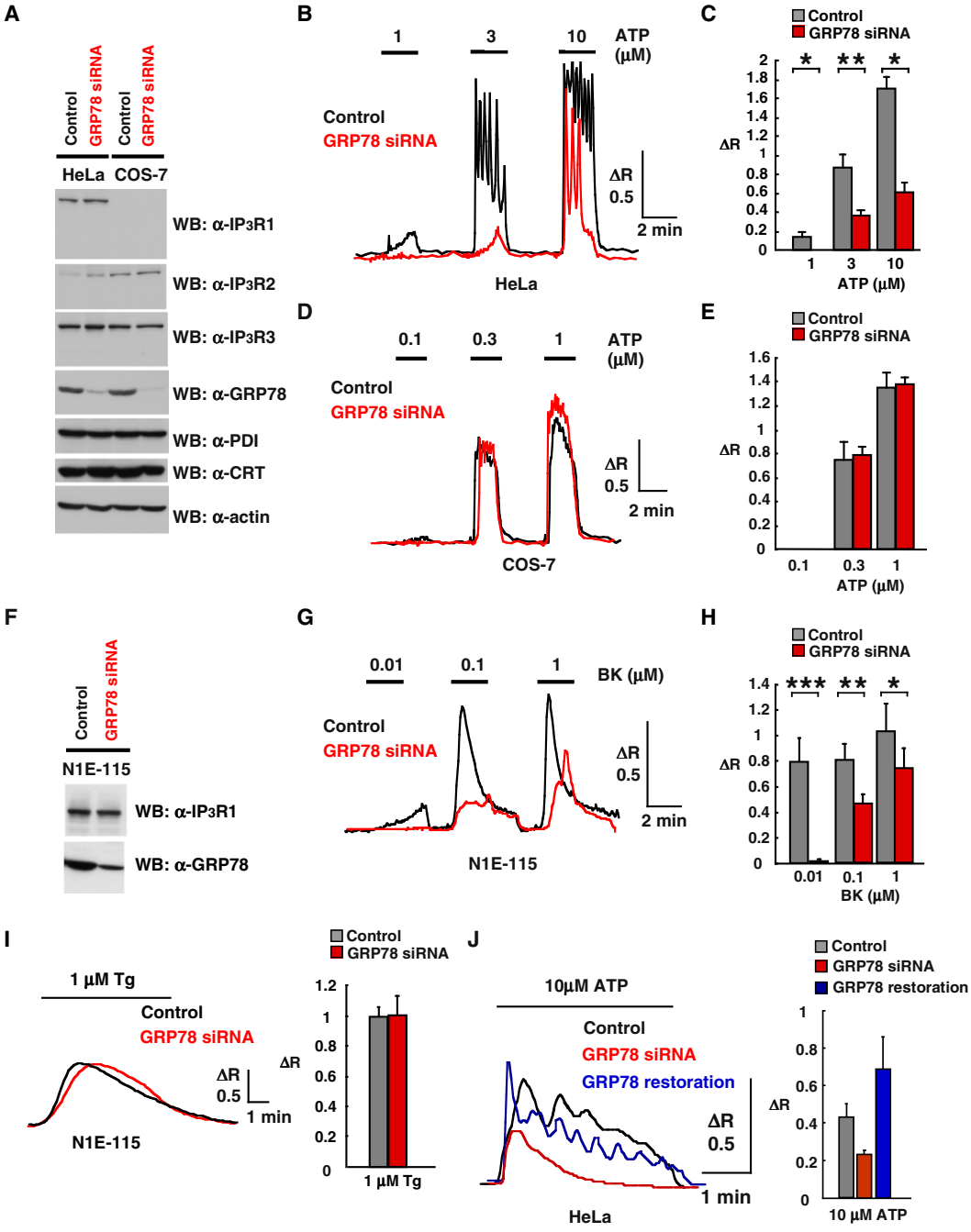

Figure 5. GRP78 Knockdown Inhibits IP_3R1-Mediated Ca^{2+} Release

(A) Knockdown of GRP78 in HeLa and COS-7 cells. The detergent-solubilized fractions of HeLa and COS-7 cells transfected with siRNAs were analyzed by western blotting with the antibodies for IP_3R1, IP_3R2, IP_3R3, GRP78, protein disulfide isomerase (PDI), calreticulin (CRT), and actin.

(B and C) Knockdown of GRP78 inhibits Ca^{2+} release in HeLa cells. (B) Seventy-two to ninety-six hours after siRNA transfection, cells were stimulated with 1, 3, and 10 μM ATP in the presence of extracellular Ca^{2+}. (C) The average peak amplitude was significantly lower in GRP78 siRNA-transfected cells (red) (0.004 ± 0.001 [1 μM], 0.36 ± 0.06 [3 μM], 0.62 ± 0.1 [10 μM]) than in the control cells (gray) (0.15 ± 0.05 [1 μM], 0.88 ± 0.13 [3 μM], 1.71 ± 0.12 [10 μM]).

(D) Seventy-two hours after siRNA transfection, COS-7 cells were stimulated with 0.1, 0.3, and 1 μM ATP in the presence of extracellular Ca^{2+}.

(E) Average peak amplitude of the Ca^{2+} response in COS-7 cells transfected with control siRNA (gray) (0.74 ± 0.15 [0.3 μM], 1.35 ± 0.12 [1 μM]) or GRP78 siRNA (red) (0.79 ± 0.07 [0.3 μM], 1.38 ± 0.04 [1 μM]).

(F) Knockdown of GRP78 in N1E-115 cells. The soluble fractions of N1E-115 cells transfected with indicated siRNA were analyzed as in (A).

(G) Seventy-two hours after siRNA transfection, N1E-115 cells were stimulated with 0.01, 0.1, and 1 μM bradykinin (BK) in the presence of extracellular Ca^{2+}.

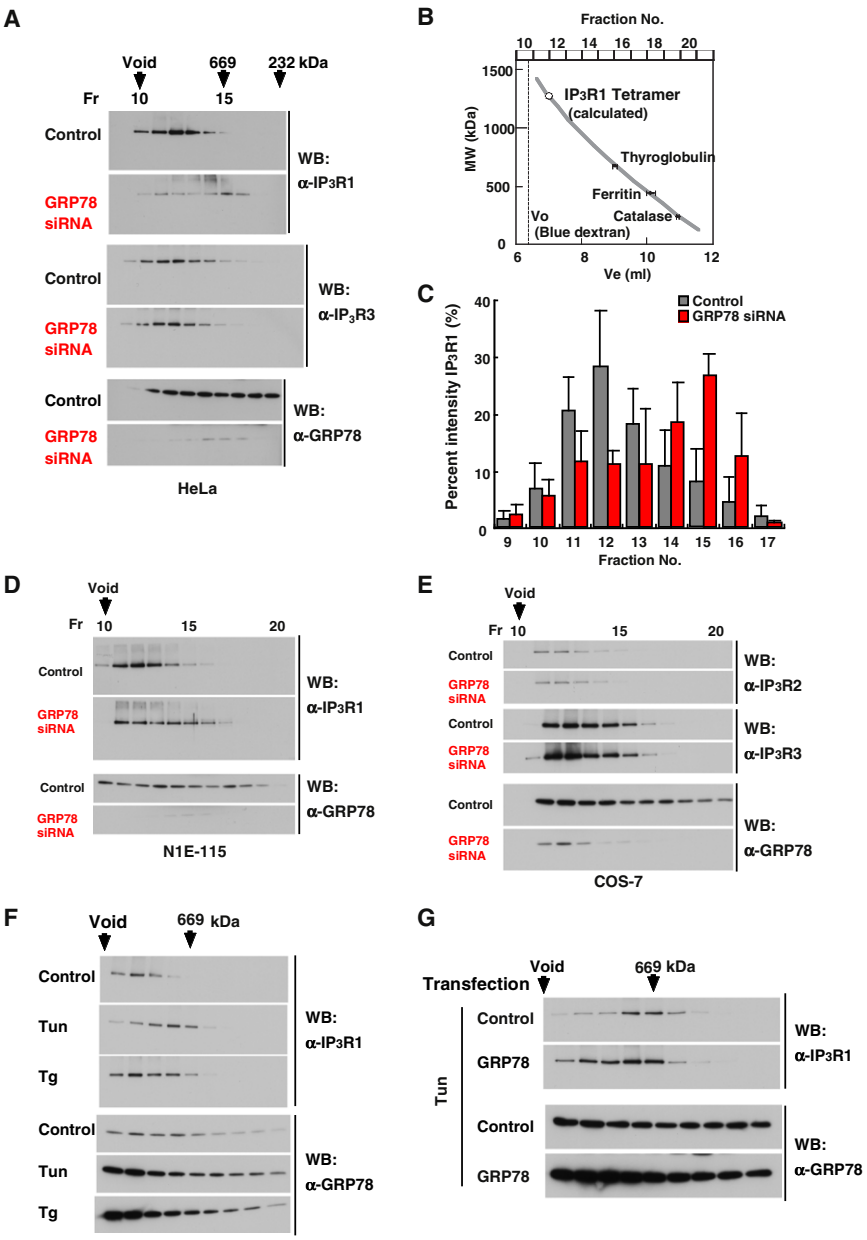

Figure 6. GRP78 Knockdown Impairs IP_3R1 Assembly

(A) HeLa cells transfected with control siRNA or GRP78 siRNA for 96 hr were crosslinked with DSP and the soluble fractions were subjected to gel filtration. Resulting fractions were analyzed by western blotting with indicated antibodies. Exclusion volume of molecular size markers is shown at the top of the panel (A).

(B) Calibration of elution profiles of gel filtration. Vo is the void volume of the column estimated with blue dextran 2000 and Ve is the elution volumes of the proteins.

(C) Quantified levels of IP_3R1 in gel filtration fractions from three independent experiments using western blotting analysis.

(D and E) Gel filtration was performed using the soluble fractions of N1E-115 (D) and COS-7 cells (E) as in (A). Resulting fractions were analyzed as in (A).

(F) HeLa cells were treated with control (DMSO), Tun (4 μg/ml), or Tg (2 μM) for 16 hr. After crosslinking with DSP, the detergent-solubled cell lysates were subject to FPLC. The resultant fractions were analyzed by western blotting.

(G) GRP78 overexpression ameliorates ER stress-dependent impairment of IP_3R1 assembly. Thirty-six hours after transfection with a vector for control or Myc-GRP78 in HeLa cells, the cells were treated with control DMSO or Tun and then were analyzed as described above.

See also Figure S5.

ATP supply into ER and subsequently impairs functional IP_3R1-GRP78 interaction that depends on ATP. Impaired function of IP_3R1 was also observed in the cerebellum of the model mice, which may contribute to the understanding of the pathology of early-onset HD, in which patients frequently show cerebellar atrophy, widespread Purkinje cell loss (Seneca et al., 2004; Sakazume et al., 2009), and other motor disorders associated with altered Ca^{2+} mobilization, ER stress, and mitochondrial dysfunction (Schröder and Kaufman, 2005; Kim et al., 2008).

Our results also demonstrate the influential role of GRP78 in IP_3R subunit assembly. In addition to results of direct assessments of the assembly status of IP_3R1, this role of GRP78 is further strengthened by findings indicating the irrelevant roles of GRP78 in IP_3R1 folding and degradation. First,

(H) The average peak amplitude was significantly lower in GRP78 siRNA-transfected cells (red) (0.02 ± 0.02 [0.01 μM], 0.46 ± 0.08 [0.1 μM], 0.74 ± 0.16 [1 μM]) than in the control cells (gray) (0.79 ± 0.19 [0.01 μM], 0.81 ± 0.13 [0.1 μM], 1.03 ± 0.22 [1 μM]).

(I) Knockdown of GRP78 did not decrease ER Ca^{2+} content in N1E-115 cells. (Left) Cells were stimulated with 1 μM Tg in the absence of extracellular Ca^{2+}. (Right) The average peak amplitudes in control siRNA- and GRP78 siRNA-transfected cells were 0.97 ± 0.05 and 0.98 ± 0.13, respectively. Representative Ca^{2+} responses in control siRNA-transfected (black) or GRP78 siRNA-transfected cells (red) are shown in (B), (D), (G), and (I).

(J) GRP78 re-expression restored attenuated IP_3R1-mediated Ca^{2+} release. HeLa cells were first transfected with siRNA against the GRP78 3′UTR. Forty-eight hours after transfection, the cells were transfected with expression vectors for monomeric RFP (red) and full-length (blue) GRP78. Similarly, HeLa cells were transfected with control siRNA and control vectors (black). Forty-eight hours after the second transfection, the cells were stimulated with 10 μM ATP in nominally Ca^{2+}-free medium. Representative Ca^{2+} responses (left) and the average peak amplitudes (right) are shown. Data in (C), (E), (H), (I), and (J) are presented as mean ± SEM from at least three independent experiments. *p < 0.05; **p < 0.01; ***p < 0.001.

See also Figure S4.

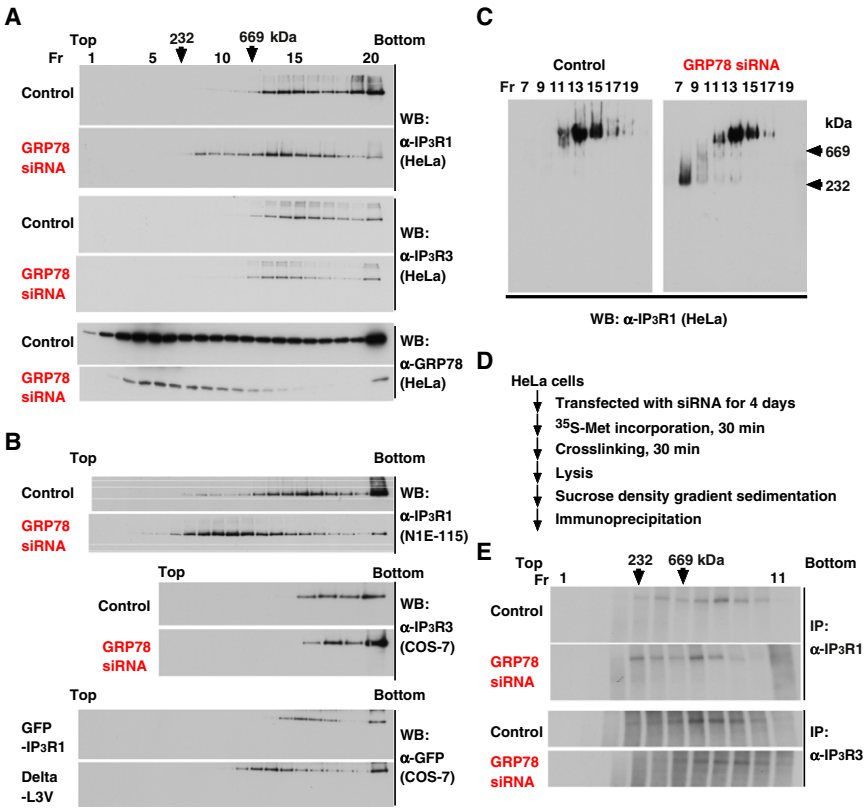

Figure 7. GRP78 Knockdown Inhibits the Tetrameric Assembly of Newly Synthesized IP_3R1

(A and B) HeLa, N1E-115, and COS-7 cells transfected with indicated siRNA, GFP-IP_3R1, or GFP-IP_3R1-deltaL3V were solubilized and then subjected to sedimentation in a linear 5%–20% sucrose gradient. Fractions were collected from top to bottom and analyzed by western blotting with indicated antibodies.

(C) HeLa cells were transfected with control siRNA (left panel) or GRP78 siRNA (right panel), and then crosslinked with a noncleavage crosslinker, disuccinimidylsuberate (DSS). The soluble fractions were subjected to sedimentation in a linear 5%–20% sucrose gradient and resulting fractions were separated on native-PAGE in the absence of both SDS and a reducing agent. Migration of molecular size markers is shown at right panel.

(D) Experimental procedure of pulse labeling.

(E) The IP samples were separated in SDS-PAGE and detected by autoradiography. The representative results of IP with α-IP_3R1 and α-IP_3R3 are shown from three and two independent experiments, respectively.

GRP78 knockdown did not cause misfolding-dependent retrodegradation or aggregation of IP_3R1. Second, GRP78 knockdown did not affect N-linked glycosylation, supporting that IP_3R1 is normally folded by the ER lectin chaperone calnexin (Joseph et al., 1999; Ellgaard and Helenius, 2003) and that IP_3R1 does not undergo disassembly-dependent degradation (Khan and Joseph, 2003). Third, the specific binding behavior of GRP78 to IP_3R1 is incompatible with typical binding behaviors of GRP78 to unfolded substrates regarding the dissociation kinetics and the preferences of ATP and ADP (Misselwitz et al., 1998; Hendershot, 2004; Nawa et al., 2007). Therefore, our findings strongly support the argument that GRP78 functions as an assembler of IP_3R1.

Here, we propose a molecular mechanism for IP_3R subunit assembly in which GRP78 interacts with nascent IP_3R1 monomers and tethers them to ensure the fidelity of subunit assembly without stochastic misassembly. It has rarely been considered that chaperones function as assemblers of oligomeric complexes, whereas emerging literature has begun to clarify the role of nuclear chaperones in nucleosome assembly (Ellis, 2006) and the requirement of cystolic chaperones for mammalian proteasome assembly (Hirano et al., 2005). Given that all intracellular ion channels undergo biogenetic processes including membrane insertion in ER (Deutsch, 2003), our findings may suggest general mechanisms in which ER chaperones regulate quaternary structures of ion channels. Our results also indicate an energy-dependent tetrameric assembly of IP_3R1 by GRP78, which sheds new light on the subunit assembly of ion channels including IP_3R, which has been thought to spontaneously occur depending on their physical properties (Deutsch, 2003).

Our results indicate that L3Vs have several reliable characteristics allowing it to serve as the recognition domain, responsible for the tetramer formation, and these results highlight the significances of the short domains L3Vs in the subunit assembly of IP_3Rs. First, L3Vs are exposed to the lumenal space, allowing ER chaperones that can function as assemblers to recognize them. Second, the sequence diversity of L3Vs enables the subtype-specific associated proteins (chaperones) to selectively determine the subunit assembly. In contrast, the conserved regions of L3Cs allow chromogranins to bind to all subtypes of IP_3Rs (Yoo and Lewis, 2000; Yoo, 2010), suggesting that L3Cs exert their roles in the nonselective subunit assembly. Finally, the location immediately before L3C would be suitable to monitor and to ensure subsequent arrangement of the pore-loop, TM5, and TM6 helixes without misarrangement. Many ion channels of other tetrameric channels contain six TMs, such as Kv channels, cyclic nucleotide-gated channels, and transient receptor potential channels, and have a third large loop that forms an ion-permeating pore (Ashcroft, 2006) that corresponds to L3 of IP_3Rs. A conceptually similar mechanism could be applied to these channels including other IP_3R subtypes. It should be noted that our finding is consistent with previous studies which used a series of deletion constructs of IP_3R1 and in vitro translation system demonstrating that L3 is important for the tetramer formation (Galvan et al., 1999; Parker et al., 2004) and further accounts for preferred subunit interaction rather than random association and subtype-dependent kinetics of synthesis (Joseph et al., 2000).

Our findings also provide a new explanation for subtype-specific regulation of IP_3Rs. Many proteins have been identified

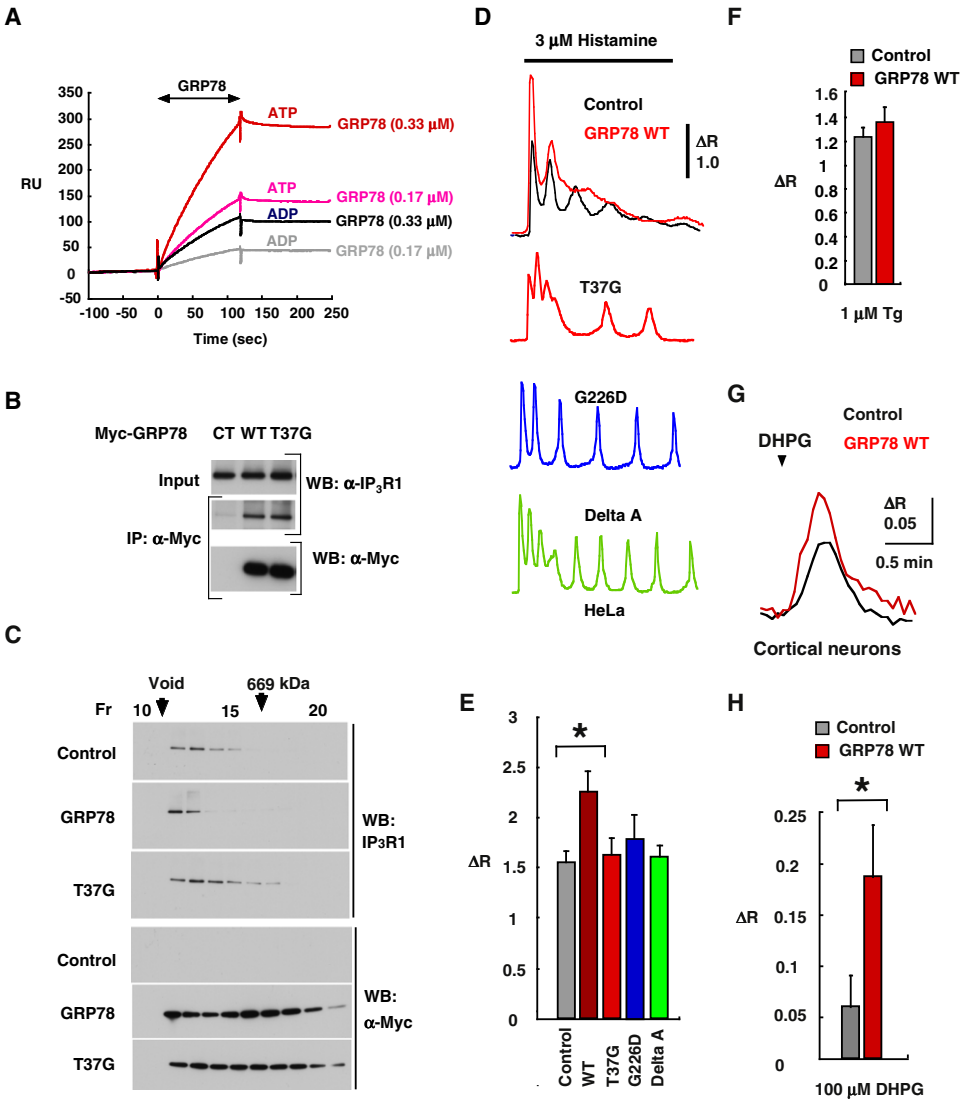

Figure 8. GRP78 Regulates the IP_3R1 Assembly Depending on Its ATPase

(A) ATP-dependent binding behavior of GRP78 to 1L3V. 1,500 resonance unit (RU) of GST-1L3V were immobilized. At time 0, a solution containing the indicated concentration of GRP78 was introduced and passed over the chip for 120 s. Association and dissociation were followed in the presence of 5 mM ATP or ADP. The association kinetics between GRP78 and GST-1L3V ($k_{on} = 8.6 \times 10^3$ [$M^{-1}s^{-1}$]) and the dissociation kinetics of GRP78 from 1L3V ($k_{off} = 3.6 \times 10^{-4}$ [s^{-1}] and Kd = 4.49×10^{-8} [M]) in the presence of ATP are obtained from three independent experiments.

(B) HeLa cells were transfected with vectors for WT or an ATPase mutant of GRP78, T37G. Using the lysates, IP was performed with α-Myc. The lysates (Input) and IP samples were analyzed by western blotting with α-IP_3R1 (top and middle) or α-Myc (bottom).

(C) HeLa cells were transfected with vectors for WT or an ATPase mutant of GRP78, T37G. After crosslinking with DSP, the detergent-solubled cell lysates were subject to FPLC. The resultant fractions were analyzed by western blotting.

(D) HeLa cells were cotransfected with vectors for RFP-KDEL and GRP78 ATPase mutants. Forty-eight hours after transfection, the cells were stimulated with 3 μM histamine in the absence of extracellular Ca^{2+}. Representative Ca^{2+} responses in RFP-positive cells are shown.

(E) The average peak amplitudes were 1.56 ± 0.10 (control), 2.26 ± 0.20, (GRP78 WT), 1.62 ± 0.17 (T37G), 1.80 ± 0.23 (G226D), and 1.60 ± 0.11 (Delta A). Results are mean ± SEM from at least three independent experiments. *$p < 0.05$.

(F) The Ca^{2+} storage capacity is unchanged in HeLa cells expressing GRP78. Quantification of the peak amplitude in cells stimulated with 1 μM Tg.

(G and H) Primary cortical neurons were cotransfected with expression vectors for monomeric RFP and GRP78 WT. Forty-eight hours after transfection, the cells were stimulated with 100 μM DHPG, followed by depolarization with 30 mM KCl to fill the Ca^{2+} store. (G) Representative Ca^{2+} responses in RFP-positive cells are shown. (H) The average peak amplitudes were 0.053 ± 0.03 (control) and 0.184 ± 0.052 (GRP78 WT). Data are presented mean ± SEM from six independent experiments. *$p < 0.05$.

See also Figure S6.

to regulate IP_3R1 in a subtype-specific manner (Mikoshiba, 2007), but the mechanisms by which the interaction generates the activatory or inhibitory status of IP_3Rs at quaternary structural level remain elusive. Our study first demonstrates a molecular mechanism in which IP_3R1 is subtype specifically regulated by controlling subunit assembly and furthermore suggests analogous mechanisms for other subtypes of IP_3Rs. Importantly, GRP78 facilitate IP_3R1 assembly by its binding to 1L3V under oxidized conditions that mimic the ER lumen (Figure S6). On the other hand, another ER chaperone ERp44 inhibits IP_3R1 by its binding to 1L3V under reduced conditions (Higo et al., 2005). Under normal (oxidized) conditions, GRP78 inhibits ERp44-binding to 1L3V. Altogether, these suggest that GRP78 makes IP_3R1 shift to the activated (or ready) state by facilitating the subunit assembly and by preventing the ERp44-dependent inhibition of the channel activity under normal ER conditions. In other words, 1L3V works as a key domain to switch the activation status of IP_3R1 by changing its binding partners depending on the redox states in ER.

In summary, our data show that IP_3R1 senses ER stress through GRP78 to alter the Ca^{2+} signal and affect cell fate. Based on our data that the functional interaction between IP_3R1 and GRP78 is impaired during ER stress and in the HD model, we propose that IP_3R1 functions as a signal integrator to link ER stress with Ca^{2+} signaling to regulate neuronal cell death implicated in neurodegenerative diseases.

EXPERIMENTAL PROCEDURES

Reagents

Tunicamycin, thapsigargin, bradykinin, and histamine were purchased from Sigma. Dithiothreitol (DTT) was obtained from Wako. Dithiobis (succinimidyl) propionate (DSP) and disuccinimidylsuberate (DSS) were purchased from Pierce. ATP was from GE Healthcare. 3,5-dihydroxyphenylglycine (DHPG) was purchased from Tocris.

Constructs

See Supplemental Information.

Animal Experiments

IP_3R1 knockout mice were produced as described previously (Matsumoto et al., 1996) and WT littermates were intraperitoneally injected with 1 μg/g Tun or control PBS, then anesthetized 2 days later and transcardially perfused with PBS containing 4% paraformaldehyde. The brain slices were subjected to hematoxylin and eosin (HE) staining or to immunostaining with mouse monoclonal antibody against calbindin. All animals were ethically treated according to the guideline of Animal Experiments Committee of RIKEN Brain Science Institute.

Cell Culture and Transfection

HeLa, COS-7, and N1E-115 cells were cultured in Dulbecco's modified Eagle medium supplemented with 10% heat-inactivated fetal bovine serum, 100 U/ml penicillin, and 100 μg/ml streptomycin. Transfections of siRNAs and expression vectors were performed using Lipofectamine2000 (Invitrogen) or TransIT (Mirus), respectively, according to the manufacturers' instructions.

Short Interfering RNA

Scrambled short interfering RNA (siRNA) cocktails against human GRP78, the negative control cocktail, siRNA against mouse GRP78, and the control mouse siRNA were purchased from B-Bridge International, Inc. The DNA target sequences for human GRP78 were CGTTCAAGGTGGTTGAAAA, GAATCAGA TTGGAGATAAA, and AGAAAAGAGTCCAGGTAAA. Control sequences were ATCCGCGCGATAGTACGTA, TTACGCGTAGCGTAATACG, and TATTCGCG CGTATAGCGGT. DNA target sequence for mouse GRP78 was GTCTCGA ATGTAATTGGAA. DNA target sequence for human IP_3R1 was TGAGACAGA AAACAGGAAA. Control sequence was TAGCGACTAAACACATCAA. SiRNA duplexes were resolved in water to a final concentration of 25 μM.

Apoptosis Analysis and Mitochondrial Membrane Potential

Apoptosis was assessed by Annexin-V/propidium iodide (PI) staining. HeLa cells were transfected with IP_3R1 siRNA for 48 hr and then treated with Tun (5 μg/ml) or Tg (2 μM) or DTT (2 mM) for 12, 24, or 48 hr. The cells were collected and stained with Annexin-V fluoroscein isothiocyanate (FITC)/PI (BioVision) for 5 min at RT. The percentage of apoptosis (Annexin-positive/PI-negative) was determined by flow cytometer analysis, in which the cells treated with 1 μM staurosporine for 4 hr were used as positive controls.

Apoptosis was also evaluated by the disruption of the mitochondrial inner-membrane electrochemical potential using a fluorescent cationic dye, MitoCapture (BioVision). In healthy cells, MitoCapture accumulates in the mitochondria as punctate red fluorescence that is detectable using the PI channel (FL2). In contrast, in apoptotic cells, the altered mitochondrial membrane potential causes the dye to disperse into the cytoplasm and remains in its monomer form, generating a green fluorescence that is detectable using the FITC channel (FL1). HeLa cells transfected with IP_3R1 siRNA were treated with ER stressors described above and then collected to stain with MitoCapture (BioVision) for 20 min at 37°C. Fluorescent signals were analyzed by flow cytometer.

Ca^{2+} Measurements

Ca^{2+} imaging was performed using cultured cells as previously described (Higo et al., 2005). In brief, cells were incubated for 30 min with a Ca^{2+} indicator, 5 μM fura-2 acetoxymethyl-ester (Dojindo). Cells were perfused with balanced salt solution (115 mM NaCl, 5.4 mM KCl, 1 mM $MgCl_2$, 10 mM glucose, 20 mM HEPES [pH 7.4], and either 2 mM $CaCl_2$ or nominally Ca^{2+} free). Image capture and processing were performed with an Argus 50/CA system (Hamamatsu Photonics) at RT. Delta R (F340/F380) is the change in the ratio of the fluorescent intensities of fura-2 that are excited by light at a wavelength of 340 and 380 nm (F340 and F380), which is generally used for assessing the intracellular Ca^{2+} concentration.

For in vitro Ca^{2+} measurements, microsomal membrane vesicles obtained from cultured cells or mice cerebella were mixed with 0.2 μM fura-2 in a cuvette. IP_3-induced Ca^{2+} release was measured using an F-2500 spectrofluorometer (Hitachi, Japan).

Primary Cell Cultures and Transfection

Primary neurons were isolated and cultured as described (Deyts et al., 2009) with some modifications. For complete experimental details, see Supplementary Information.

Identification of GRP78

See Supplemental Information.

GST Pull-Down, Immunoprecipitation, Western Blot Assays

These biochemical assays were performed as previously described (Higo et al., 2005). For complete experimental details, see Supplemental Information.

Immunocytochemistry and Immunohistochemistry

See Supplemental Information.

Gel Filtration

Size exclusion chromatography was performed at 4°C on a Tosoh TSK G4000SWXL column (30 cm × 7.8 mm i.d.). The pre-column (TSK guard column SWXL) was connected to trap sticky molecules. Columns were equilibrated with TNE buffer. The cell extract was applied onto the column via 500 μl sample loop and eluted at a flow rate of 0.5 ml/min. The exclusion volume of standard protein (GE Healthcare): thyroglobulin (669 kDa), ferritin (440 kDa), catalase (232 kDa), and the void volume, which is determined with blue dextran 2000, were completely reproducible under identical

conditions. The collected 20–30 fractions (500 μl) were resolved by SDS-PAGE and analyzed by western blotting.

Sucrose Density Gradient Sedimentation

The 1–2 ml of cell lysates were loaded on to 10 ml linear 5%–20% sucrose gradients made in TNE buffer. The gradients were centrifuged at 100,000 × g for 16 hr in a Beckman SW41 ultracentrifuge rotator at 2°C. Fractions were collected from the top to bottom of the gradients, resolved by SDS-PAGE or native-PAGE, and analyzed by western blotting.

Native-PAGE

See Supplemental Information.

Pulse Labeling

HeLa cells were cultured in methionine-free DMEM containing 5% dialyzed FBS for 2 hr prior to labeling. The cells were labeled with 50 μCi/ml [^{35}S]-methionine (Perkin-Elmer) in the methionine-free DMEM for 30 min. After extensive washing with PBS, the cells were treated with 2 mM DSP for 30 min and then solubilized in TNE buffer containing 1% Triton X-100. The cleared lysates were loaded on 5%–20% sucrose gradients and centrifuged as described above. Collected fractions were immunoprecipitated with anti-IP_3R1 or anti-IP_3R3. The IP samples were resolved by SDS-PAGE, detected by autoradiography, and analyzed by densitometry.

Surface Plasmon Resonance Experiments

Surface plasmon resonance (SPR) experiments were done on a BIAcore2000 (Biacore) using CM5 research grade chips. For complete experimental details, see Supplemental Information.

SUPPLEMENTAL INFORMATION

Supplemental Information includes six figures and Supplemental Experimental Procedures and can be found with this article online at doi:10.1016/j.neuron.2010.11.010

ACKNOWLEDGMENTS

We thank A. Mizutani for many biochemical experiments, including SPR analysis. We also thank T. Inoue and T. Michikawa for helpful discussion, and K. Nakamura, A. Terauchi, and A. Suzuki for excellent technical assistance. We thank for the support provided by the Research Resource Center at the RIKEN BSI for mass spectrometry, flow cytometry, and HE staining. This study was supported by a grant from the JST, Grants-in-Aid (T.H. and K.M.), the 21st Century COE Program, Center for Integrated Brain Medical Science, as well as the Ministry of Education, Culture, Sports, Science and Technology, Japan. We declare that none of the authors has a financial interest related to this work. We dedicate this report to Takeshi Nakamura, whose untimely death from cancer was a great loss for us.

Accepted: September 17, 2010
Published: December 8, 2010

REFERENCES

Ashcroft, F.M. (2006). From molecule to malady. Nature *440*, 440–447.

Berridge, M.J., Bootman, M.D., and Roderick, H.L. (2003). Calcium signalling: dynamics, homeostasis and remodelling. Nat. Rev. Mol. Cell Biol. *4*, 517–529.

Biagioli, M., Pifferi, S., Ragghianti, M., Bucci, S., Rizzuto, R., and Pinton, P. (2008). Endoplasmic reticulum stress and alteration in calcium homeostasis are involved in cadmium-induced apoptosis. Cell Calcium *43*, 184–195.

Blackshaw, S., Sawa, A., Sharp, A.H., Ross, C.A., Snyder, S.H., and Khan, A.A. (2000). Type 3 inositol 1,4,5-trisphosphate receptor modulates cell death. FASEB J. *14*, 1375–1379.

Boehning, D., Patterson, R.L., Sedaghat, L., Glebova, N.O., Kurosaki, T., and Snyder, S.H. (2003). Cytochrome c binds to inositol (1,4,5) trisphosphate receptors, amplifying calcium-dependent apoptosis. Nat. Cell Biol. *5*, 1051–1061.

Bossy-Wetzel, E., Petrilli, A., and Knott, A.B. (2008). Mutant huntingtin and mitochondrial dysfunction. Trends Neurosci. *31*, 609–616.

Collins, T.J., Lipp, P., Berridge, M.J., Li, W., and Bootman, M.D. (2000). Inositol 1,4,5-trisphosphate-induced Ca2+ release is inhibited by mitochondrial depolarization. Biochem. J. *347*, 593–600.

Deutsch, C. (2003). The birth of a channel. Neuron *40*, 265–276.

Deyts, C., Galan-Rodriguez, B., Martin, E., Bouveyron, N., Roze, E., Charvin, D., Caboche, J., and Bétuing, S. (2009). Dopamine D2 receptor stimulation potentiates PolyQ-Huntingtin-induced mouse striatal neuron dysfunctions via Rho/ROCK-II activation. PLoS ONE *4*, e8287. 10.1371/journal.pone.0008287.

Ellgaard, L., and Helenius, A. (2003). Quality control in the endoplasmic reticulum. Nat. Rev. Mol. Cell Biol. *4*, 181–191.

Ellis, R.J. (2006). Molecular chaperones: assisting assembly in addition to folding. Trends Biochem. Sci. *31*, 395–401.

Fink, C.C., Slepchenko, B., Moraru, I.I., Watras, J., Schaff, J.C., and Loew, L.M. (2000). An image-based model of calcium waves in differentiated neuroblastoma cells. Biophys. J. *79*, 163–183.

Galvan, D.L., Borrego-Diaz, E., Perez, P.J., and Mignery, G.A. (1999). Subunit oligomerization, and topology of the inositol 1,4, 5-trisphosphate receptor. J. Biol. Chem. *274*, 29483–29492.

Gaut, J.R., and Hendershot, L.M. (1993). Mutations within the nucleotide binding site of immunoglobulin-binding protein inhibit ATPase activity and interfere with release of immunoglobulin heavy chain. J. Biol. Chem. *268*, 7248–7255.

Hara, K., Shiga, A., Nozaki, H., Mitsui, J., Takahashi, Y., Ishiguro, H., Yomono, H., Kurisaki, H., Goto, J., Ikeuchi, T., et al. (2008). Total deletion and a missense mutation of ITPR1 in Japanese SCA15 families. Neurology *71*, 547–551.

Hattori, M., Suzuki, A.Z., Higo, T., Miyauchi, H., Michikawa, T., Nakamura, T., Inoue, T., and Mikoshiba, K. (2004). Distinct roles of inositol 1,4,5-trisphosphate receptor types 1 and 3 in Ca2+ signaling. J. Biol. Chem. *279*, 11967–11975.

Hendershot, L.M. (2004). The ER function BiP is a master regulator of ER function. Mt. Sinai J. Med. *71*, 289–297.

Hetz, C., Bernasconi, P., Fisher, J., Lee, A.H., Bassik, M.C., Antonsson, B., Brandt, G.S., Iwakoshi, N.N., Schinzel, A., Glimcher, L.H., and Korsmeyer, S.J. (2006). Proapoptotic BAX and BAK modulate the unfolded protein response by a direct interaction with IRE1alpha. Science *312*, 572–576.

Higo, T., Hattori, M., Nakamura, T., Natsume, T., Michikawa, T., and Mikoshiba, K. (2005). Subtype-specific and ER lumenal environment-dependent regulation of inositol 1,4,5-trisphosphate receptor type 1 by ERp44. Cell *120*, 85–98.

Hirano, Y., Hendil, K.B., Yashiroda, H., Iemura, S., Nagane, R., Hioki, Y., Natsume, T., Tanaka, K., and Murata, S. (2005). A heterodimeric complex that promotes the assembly of mammalian 20S proteasomes. Nature *437*, 1381–1385.

Joseph, S.K., and Hajnóczky, G. (2007). IP3 receptors in cell survival and apoptosis: Ca^{2+} release and beyond. Apoptosis *12*, 951–968.

Joseph, S.K., Boehning, D., Bokkala, S., Watkins, R., and Widjaja, J. (1999). Biosynthesis of inositol trisphosphate receptors: selective association with the molecular chaperone calnexin. Biochem. J. *342*, 153–161.

Joseph, S.K., Bokkala, S., Boehning, D., and Zeigler, S. (2000). Factors determining the composition of inositol trisphosphate receptor hetero-oligomers expressed in COS cells. J. Biol. Chem. *275*, 16084–16090.

Khan, M.T., and Joseph, S.K. (2003). Proteolysis of type I inositol 1,4,5-trisphosphate receptor in WB rat liver cells. Biochem. J. *375*, 603–611.

Kim, I., Xu, W., and Reed, J.C. (2008). Cell death and endoplasmic reticulum stress: Disease relevance and therapeutic opportunities. Nat. Rev. Drug Discov. *7*, 1013–1030.

Li, J., Lee, B., and Lee, A.S. (2006). Endoplasmic reticulum stress-induced apoptosis: Multiple pathways and activation of p53-up-regulated modulator of apoptosis (PUMA) and NOXA by p53. J. Biol. Chem. *281*, 7260–7270.

Lin, J.H., Li, H., Yasumura, D., Cohen, H.R., Zhang, C., Panning, B., Shokat, K.M., Lavail, M.M., and Walter, P. (2007). IRE1 signaling affects cell fate during the unfolded protein response. Science *318*, 944–949.

Matassa, A.A., Carpenter, L., Biden, T.J., Humphries, M.J., and Reyland, M.E. (2001). PKCdelta is required for mitochondrial-dependent apoptosis in salivary epithelial cells. J. Biol. Chem. *276*, 29719–29728.

Matsumoto, M., Nakagawa, T., Inoue, T., Nagata, E., Tanaka, K., Takano, H., Minowa, O., Kuno, J., Sakakibara, S., Yamada, M., et al. (1996). Ataxia and epileptic seizures in mice lacking type 1 inositol 1,4,5-trisphosphate receptor. Nature *379*, 168–171.

Mendes, C.C., Gomes, D.A., Thompson, M., Souto, N.C., Goes, T.S., Goes, A.M., Rodrigues, M.A., Gomez, M.V., Nathanson, M.H., and Leite, M.F. (2005). The type III inositol 1,4,5-trisphosphate receptor preferentially transmits apoptotic Ca2+ signals into mitochondria. J. Biol. Chem. *280*, 40892–40900.

Mikoshiba, K. (2007). IP3 receptor/Ca^{2+} channel: From discovery to new signaling concepts. J. Neurochem. *102*, 1426–1446.

Mimura, N., Hamada, H., Kashio, M., Jin, H., Toyama, Y., Kimura, K., Iida, M., Goto, S., Saisho, H., Toshimori, K., et al. (2007). Aberrant quality control in the endoplasmic reticulum impairs the biosynthesis of pulmonary surfactant in mice expressing mutant BiP. Cell Death Differ. *14*, 1475–1485.

Misselwitz, B., Staeck, O., and Rapoport, T.A. (1998). J proteins catalytically activate Hsp70 molecules to trap a wide range of peptide sequences. Mol. Cell *2*, 593–603.

Nawa, D., Shimada, O., Kawasaki, N., Matsumoto, N., and Yamamoto, K. (2007). Stable interaction of the cargo receptor VIP36 with molecular chaperone BiP. Glycobiology *17*, 913–921.

Panov, A.V., Gutekunst, C.-A., Leavitt, B.R., Hayden, M.R., Burke, J.R., Strittmatter, W.J., and Greenamyre, J.T. (2002). Early mitochondrial calcium defects in Huntington's disease are a direct effect of polyglutamines. Nat. Neurosci. *5*, 731–736.

Parker, A.K., Gergely, F.V., and Taylor, C.W. (2004). Targeting of inositol 1,4,5-trisphosphate receptors to the endoplasmic reticulum by multiple signals within their transmembrane domains. J. Biol. Chem. *279*, 23797–23805.

Sakazume, S., Yoshinari, S., Oguma, E., Utsuno, E., Ishii, T., Narumi, Y., Shiihara, T., and Ohashi, H. (2009). A patient with early onset Huntington disease and severe cerebellar atrophy. Am. J. Med. Genet. A. *149A*, 598–601.

Schröder, M., and Kaufman, R.J. (2005). The mammalian unfolded protein response. Annu. Rev. Biochem. *74*, 739–789.

Scorrano, L., Oakes, S.A., Opferman, J.T., Cheng, E.H., Sorcinelli, M.D., Pozzan, T., and Korsmeyer, S.J. (2003). BAX and BAK regulation of endoplasmic reticulum Ca^{2+}: A control point for apoptosis. Science *300*, 135–139.

Seneca, S., Fagnart, D., Keymolen, K., Lissens, W., Hasaerts, D., Debulpaep, S., Desprechins, B., Liebaers, I., and De Meirleir, L. (2004). Early onset Huntington disease: A neuronal degeneration syndrome. Eur. J. Pediatr. *163*, 717–721.

Seong, I.S., Ivanova, E., Lee, J.M., Choo, Y.S., Fossale, E., Anderson, M., Gusella, J.F., Laramie, J.M., Myers, R.H., Lesort, M., and MacDonald, M.E. (2005). HD CAG repeat implicates a dominant property of huntingtin in mitochondrial energy metabolism. Hum. Mol. Genet. *14*, 2871–2880.

Sugawara, H., Kurosaki, M., Takata, M., and Kurosaki, T. (1997). Genetic evidence for involvement of type 1, type 2 and type 3 inositol 1,4,5-trisphosphate receptors in signal transduction through the B-cell antigen receptor. EMBO J. *16*, 3078–3088.

Thrower, E.C., Hagar, R.E., and Ehrlich, B.E. (2001). Regulation of Ins(1,4,5)P3 receptor isoforms by endogenous modulators. Trends Pharmacol. Sci. *22*, 580–586.

Vonsattel, J.P. (2008). Huntington disease models and human neuropathology: similarities and differences. Acta Neuropathol. *115*, 55–69.

Wang, M., Ye, R., Barron, E., Baumeister, P., Mao, C., Luo, S., Fu, Y., Luo, B., Dubeau, L., Hinton, D.R., and Lee, A.S. (2010). Essential role of the unfolded protein response regulator GRP78/BiP in protection from neuronal apoptosis. Cell Death Differ. *17*, 488–498.

Wei, J., Gaut, J.R., and Hendershot, L.M. (1995). In vitro dissociation of BiP-peptide complexes requires a conformational change in BiP after ATP binding but does not require ATP hydrolysis. J. Biol. Chem. *270*, 26677–26682.

Yoo, S.H. (2010). Secretory granules in inositol 1,4,5-trisphosphate-dependent Ca2+ signaling in the cytoplasm of neuroendocrine cells. FASEB J. *24*, 653–664.

Yoo, S.H., and Lewis, M.S. (2000). Interaction of chromogranin B and the near N-terminal region of chromogranin B with an intraluminal loop peptide of the inositol 1,4, 5-trisphosphate receptor. J. Biol. Chem. *275*, 30293–30300.

Zhu, L., Ling, S., Yu, X.D., Venkatesh, L.K., Subramanian, T., Chinnadurai, G., and Kuo, T.H. (1999). Modulation of mitochondrial Ca(2+) homeostasis by Bcl-2. J. Biol. Chem. *274*, 33267–33273.